3-Mercaptopropionic Acid Capped Gold Nanoclusters: Quantized Capacitance in Aqueous Media

LI, Di(李迪)   **LI, Jing-Hong***(李景虹)
State Key Laboratory of Electroanalytical Chemistry, Changchun Institute of Applied Chemistry, Chinese Academy of Sciences, Changchun, Jilin 130022, China

3-Mercaptopropionic acid monolayer protected gold nanoclusters (MPA-MPCs) were synthesized and characterized by transmission electron microscopy, UV-Vis spectroscopy, X-ray photoelectron spectroscopy and Fourier transform infrared spectroscopy. The exact value of quantized double-layer capacitance of MPCs in aqueous media was obtained by differential pulse voltammograms.

Keywords   gold nanoparticle, quantized double-layer capacitance, aqueous media

Introduction

An extensive research interest[1,2] in monolayer protected gold clusters (MPCs) has arisen ever since the milestone report of Brust *et al*.[3] The particularly interesting property of the MPCs core is its small capacitance (sub-attofarad, aF), which causes that single electron transfers to/from the core leading to readily measurable changes in its electronic potential. That is, the electrochemical charging of the MPCs core becomes a quantized process. However, usual alkanethiolate MPCs are not water-soluble, resulting in the limitation of their potent applications. Little work has been reported on the preparation of water-soluble gold MPCs[4,5] and the exact value of cluster capacitance in aqueous solution has not been obtained until now. In this article, we synthesized and characterized 3-mercaptopropionic acid (MPA) monolayer protected gold nanoparticles (MPA-MPCs),[6,7] and obtained the quantized capacitance charging in aqueous media via differential pulse voltammogram (DPV) experiment.

Experimental

Chemicals

3-Mercaptopropionic acid was purchased from Aldrich. $HAuCl_4 \cdot 4H_2O$ (A.R.), $NaBH_4$(A.R.) and KCl (A.R.) were acquired from standard source and used as received. Water was purified with Milli-Q (18.3 MΩ) water system.

Synthesis

The synthesis of MPA-MPCs was based on the reduction of tetrachloroauric acid with sodium borohydride in the presence of MPA. In brief, MPA (1.5 mmol/L) was added to a vigorously stirred tetrachloroauric acid aqueous solution of equal mole. The mixture was stirred for 15 min before the addition of 9-fold excess sodium borohydride reductant. The resultant solution quickly turned dark, indicating the presence of gold nanoparticles, and it was further stirred for another 8 h. The crude product was purified by loading it into cellulose ester dialysis membrane, placing in a 1-L beaker of water for 96 h and recharging with fresh water every 8 h to remove excess sodium ions, borohydride ions and chloride ions. Before dialysis, pH of the solution was 9 due to excess sodium borohydride and it turned to be 6 after dialysis.

Instruments

Transmission electron microscopy (TEM) was performed on a JEOL-JEM-2010 (JEOL, Japan) electron microscope operated at 200 kV. Samples for TEM were prepared by casting one drop of cluster solution (*ca*. 4 mg/mL) onto a standard carbon-coated (20—30 nm) formvar film on copper grid (230 mesh). Core size distribution for at least 100 individual clusters was obtained using Scion Image Beta 4.02.

Electrochemical measurements were carried out at CHI 832 electrochemical station (CHI Inc., USA) with a traditional three-electrode cell. The electrodes were a 0.031 cm^2 gold working electrode, an Ag/AgCl (saturated KCl) reference electrode and a Pt coil counter electrode. The working electrode was polished by 1 μ, 0.3 μ and 0.05 μ alumina polishing compounds consecutively, rinsed with excess water, ethanol and briefly sonicated prior to each experiment. The electrolyte was 0.1 mol/L KCl (purged with high pure N_2).

UV-Vis spectra of the clusters were acquired with a Cary-500 UV-Vis-NIR spectrophotometer (VARIAN, USA).

X-Ray photoelectron spectroscopy was conducted using a

VG ESCALAB MK II spectrometer (VG Scientific, UK) employing a monochromatic Mg Kα X-ray source ($h\nu = 1253.6$ eV). Peak positions were internally referenced to the C_{1s} peak at 284.6 eV.

Fourier transform infrared spectroscopy was conducted at FTS135 infrared spectroscopy (BIO-RAD, USA). Transmission spectra of the samples were obtained by forming thin transparent KBr pellet containing the interested materials.

Results and discussion

TEM *analysis*

TEM has been a favorable tool to determine the core shape and the size distribution of metal nanoparticles. The number of atoms per core tends towards .closed shell structures ("magic number") with an equilibrium truncated octahedral shape.[8] The closest core-core distance is proximately equal to the length of a single ligand, indicating the intercalation of chains between adjacent clusters.[9] Fig. 1 shows the TEM images of MPA-MPCs before and after dialysis respectively. The average core diameter was *ca.* 6.8 nm. It can be seen from the image that collectively connected particles formed partially continuous network. In Fig. 1a, small loosely packed aggregates and individual particles were observed. While in Fig. 1b, aggregation increased with few free particles observed. The aggregation could be attributed to the head-to-head H-bond between adjacent terminal carboxylic groups, leading to the formation of irregular "fractal" type structure.
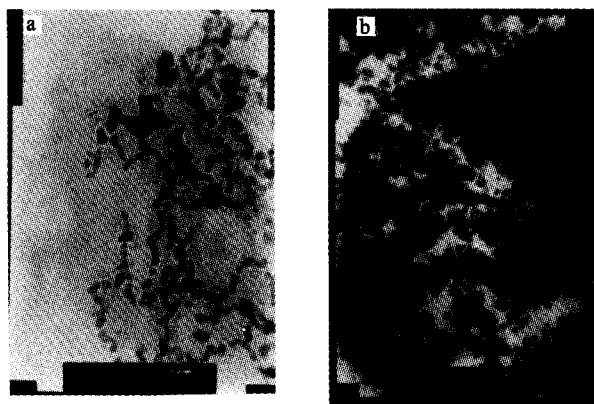

Fig. 1 TEM image of MPA-MPCs before dialysis (a) and after dialysis (b). The scale bar, 20 nm.

UV-Vis *spectroscopy*

UV-Vis spectra of the MPA-MPCs before and after dialysis are shown in Fig. 2. Metal nanoparticles exhibit strong UV-Vis absorbance, which is absent for bulk metal. It is attributed to a resonance in the collective motion of the conduction electrons in response to optical excitation, which was called localized surface plasmon resonance (SPR). The SP absorbance band of the MPA-MPCs appeared at 529 nm (be-

fore dialysis) in Fig. 2a and shifted to 536 nm (after dialysis) in Fig. 2b. For low pH, red shift of the SP band could be attributed to the aggregation of gold nanoparticles due to the formation of H-bond,[5,10] which can be seen from TEM image.
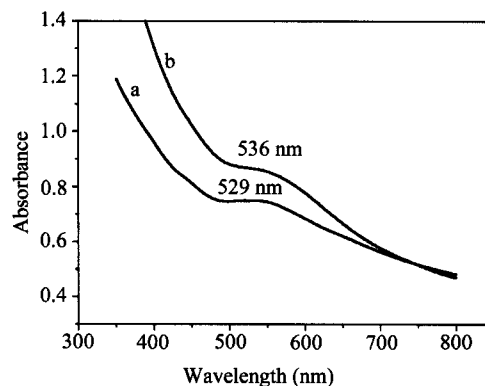

Fig. 2 UV-Vis spectra of MPA-MPCs before dialysis (a) and after dialysis (b).

XPS *analysis*

Fig. 3 gives the XPS spectra of the MPA-MPCs. Binding energy of $Au_{4f7/2}$ and S_{2p} appeared at 84.2 eV and 163.1 eV respectively. The $Au_{4f7/2}$ peak value tended to that of a surface layer of Au(I) (84.9 eV).[1] The S_{2p} binding energy
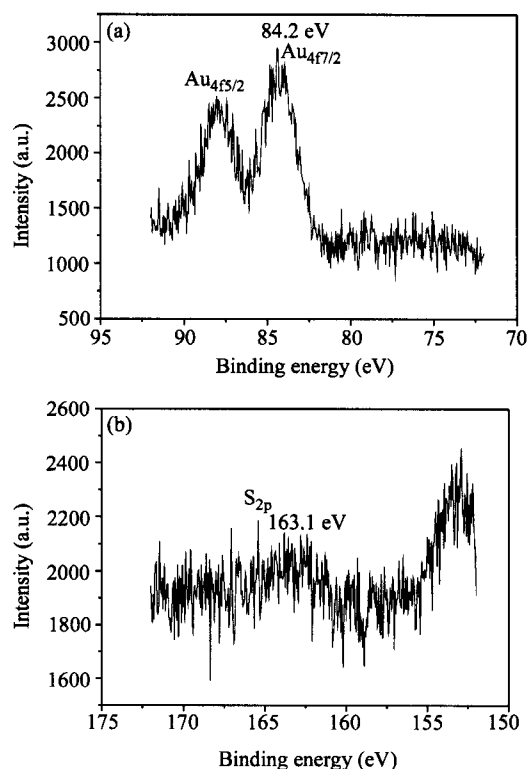

Fig. 3 XPS spectra of MPA-MPCs showing the $Au_{4f7/2}$ and S_{2p} binding energy at 84.2 eV (a) and 163.1 eV (b) respectively.

value was 162 eV for alkanethiolate ligands on flat Au surface[11](2D-SAMs) and MPCs, therefore the 163.1 eV in this experiment corresponds to a negative charge-bearing sulfur (− 2) absorbed to gold. The elemental ratio of gold to sulfur was 1.6 according to Eq. (1),[12]

$$\frac{n_{gold}}{n_{sulfur}} = \frac{I_{gold} S_{sulfur}}{I_{sulfur} S_{gold}} \qquad (1)$$

where S_{gold} and S_{sulfur} are the sensitivity factors of gold and sulfur respectively, I_{gold} and I_{sulfur} are the peak intensities of $Au_{4f7/2}$ and S_{2p} respectively.

FT-IR spectroscopy

Curves a, b and c in Fig. 4 show the mid frequency region of FT-IR spectra of free MPA, MPA-MPCs before and after dialysis respectively. Several characteristic peaks are labeled.

In the mid frequency range, the ionization of the carboxylic acid may be detected by monitoring the carboxy stretching vibration. In Fig. 4a the C = O stretch was 1710 cm^{-1} for free MPA. In this study when pH = 9 (Fig. 4b), the symmetric stretch of COO$^-$ (ν_a) in MPA-MPCs, as the form of sodium salt, was 1576 cm^{-1},[13] while its symmetric stretch (ν_s) was not well-resolved for it was overlapped with several bands [e.g., $\nu(CH_2)$ ~ 1415 cm^{-1}, $\nu(C—O)$ + $\delta(OH)$ 1430—1460 cm^{-1}]. In Fig. 4c, while for pH = 6, the ν_a and ν_s shifted to 1585 cm^{-1} and 1401 cm^{-1} respectively. The C = O stretch appeared at 1671 cm^{-1} indicating the presence of polymeric hydrogen bonding.[6] The 1621 cm^{-1} can be interpreted[14] as the C—O stretching vibration for the protonated MPA. The detection of both —COOH and —COO$^-$ species was indicative of partial protonation-deprotonation of MPA. As pH increased, the C = O stretch displayed a gradual decrease in intensity, indicating the ionization of MPA.

The results of TEM, UV-Vis and FT-IR indicated that when pH was 9 with high ionic strength, the acid was ionized to COO$^-$ Na$^+$ and the aggregation was disfavored because of repulse interactions between negatively charged carboxylate capped nanoparticles.[15] However, at low pH, when most sodium ion, borohydride ion and chloride ion had been removed by dialysis, the ionic strength decreased and ionization was weakened. Formation of H-bond between adjacent carboxylic acid groups caused the aggregation.

Differential pulse voltammograms

Quantized capacitance charging property of MPCs is an electrochemical analogue to Coulomb staircase charging[16] and may have application potentials in electronic device. In the present study, the quantized capacitance charging behavior of the MPA-MPCs was observed via DPV experiment. The clusters were not fractioned compared with the alkanethiolate-
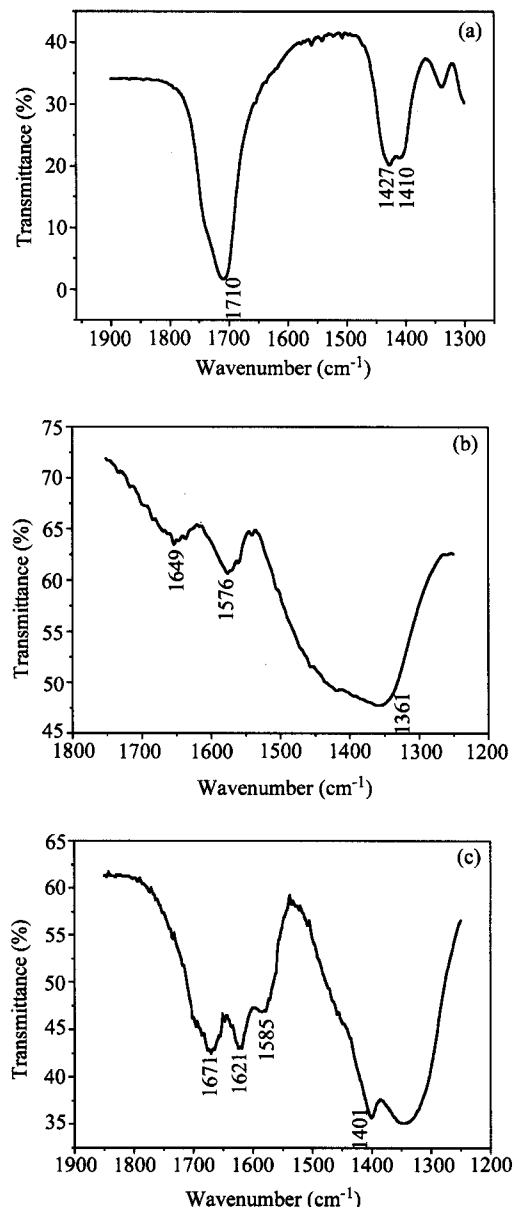

Fig. 4 Mid frequency region of FT-IR spectra of free MPA (a), MPA-MPCs before dialysis (b) and after dialysis (c).

MPCs in organic solvent.[17,18] Fig. 5 shows a series of fairly regularly spaced, one-electron transfer peaks. The consecutive (one-electron) double-layer charging peaks are formally analogous to current peaks observed in traditional redox reactions. The spacing (ΔV) is controlled by the capacitance per cluster (C_{CLU}) according to the simple relation $\Delta V = e / C_{CLU}$, where e is the electronic charge. In our work, the capacitance value of MPA capped gold cluster was 0.43 aF.

The theoretical value of C_{CLU} could be calculated according to concentric conducting spheres model,[17]

$$C_{CLU} = 4\pi\varepsilon_0\varepsilon(r/d)(r + d) \qquad (2)$$

where C_{CLU} is the cluster capacitance, ε_0 the permitivity of free space, ε the dielectric constant of the capping monolay-
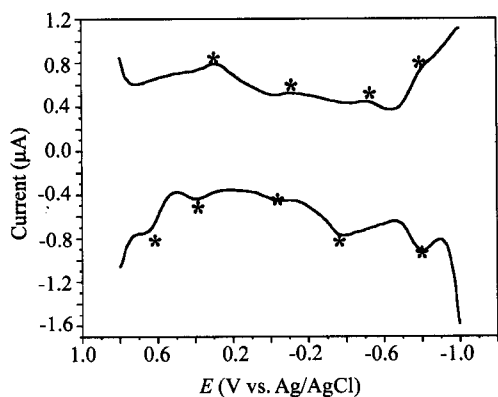
Fig. 5 Differential pulse voltammogram (DPV) of MPA-MPCs in 0.1 mol/L KCl. Concentration: ca. 2 mmol/L. Working electrode: gold disk electrode (0.031 cm^2). Reference electrode: Ag/AgCl. Counter electrode: Pt coil. DPV parameters: pulse amplitude, 80 mV; pulse width, 50 ms; pulse period, 100 ms.

er, r the radius of the core, and d the chain length of the monolayer. 0.43 aF of the MPA-MPCs corresponds to a core ridus of 0.8 nm. Thus the quantized capacitance charging reflected the attribution from fraction of very small gold nanoparticles.

The formal potentials for successive quantized double layer capacitance chargings, $Z/Z - 1$, can be shown to vary with charge state as,[17]

$$E^0_{Z, Z-1} = E_{pzc} + (Z - 1/2) e / C_{CLU} \qquad (3)$$

where $E^0_{Z, Z-1}$ is the formal potential of the $Z(Z - 1)$ charge state, which is obtained from DPV peak potentials. E_{pzc} is the potential of zero charge with the value of ca. -0.2 V (vs. Ag/AgCl).[19] Fig. 6 shows the formal potential of charging events depending on the charge state. There is a good linear relationship between the charge state and the formal potential.
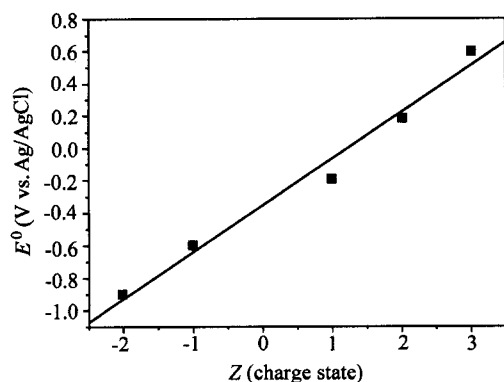

Fig. 6 Plot of formal potentials of charging events versus cluster charge state (Z).

Conclusion

MPA capped gold nanoparticles with average core size of

6.8 nm and narrow size distributions were synthesized. pH dependence of the ionization of MPA-MPCs was studied by TEM, UV-Vis and FT-IR. The results showed that aggregation of the MPA-MPCs was more serious in low pH than in high pH, being attributed to H-bond formation between adjacent carboxylic groups. The quantized double-layer capacitance of MPA capped gold nanoparticles in aqueous media was 0.43 aF, reflecting the main attribution from the fraction of very small nanoparticles.

References

1   Hostetler, M. J.; Wingate, J. E.; Zhong, C. J.; Harries, J. E.; Vachet, R. W.; Clark, M. R.; Londono, J. D.; Green, S. J.; Stokes, J. J.; Wignall, G. D.; Glish, G. L.; Porter, M. D.; Evans, N. D.; Murray, R. W. Langmuir **1998**, 14, 17.

2   Chen, S. W.; Murray, R. W. Langmuir **1999**, 15, 682.

3   Brust, M.; Walker, M.; Bethell, D.; Schiffrin, D. J.; Whyman, R. J. Chem. Soc., Chem. Commun. **1994**, 801.

4   Templeton, A. C.; Chen, S. W.; Gross, S. M.; Murray, R. W. Langmuir **1999**, 15, 66.

5   Chen, S. W. Langmuir **1999**, 15, 7551.

6   Chen, S. H.; Kimura, K. Langmuir **1999**, 15, 1075.

7   Liu, S. T.; Zhu, T.; Wang, Y. C.; Liu, Z. F. Mol. Cryst. Liq. Cryst. **1999**, 337, 245.

8   Whetten, R. L.; Shafigulin, M. N.; Khoury, J. T.; Alvarez, M. M.; Wilkinson, A. Acc. Chem. Res. **1999**, 32, 397.

9   Whetten, R. L.; Khoury, J. T.; Alvarez, M. M.; Murthy, S.; Vezmar, I.; Wang, Z. L.; Stephens, P. W.; Cleveland, C. L.; Luedtke, W. D.; Landman, U. Adv. Mater. **1996**, 8, 428.

10   Zheng, J.; Stevenson, M. S.; Hikida, R. S.; Van Patten, P. G. J. Phys. Chem. B **2002**, 106, 1252.

11   Bain, C. D.; Biebuyck, H. A.; Whitesides, G. M. Langmuir **1989**, 5, 723.

12   Bourg, M. C.; Badia, A.; Lennox, R. B. J. Phys. Chem. B **2000**, 104, 6562.

13   Zheng, W. X.; Maye, M.; Leibowitz, F. L.; Zhong, C. J. Anal. Chem. **2000**, 72, 2190.

14   Snyder, R. G.; Strauss, H. L.; Elliger, C. A. J. Phys. Chem. **1982**, 86, 5145.

15   Simard, J.; Briggs, C.; Boal, A. K.; Rotello, V. M. Chem. Commun. **2000**, 1943.

16   Gou, L.; Leobandung, E.; Chou, S. Y. Science **1997**, 275, 649.

17   Chen, S. W.; Murray, R. W.; Feldberg, S. W. J. Phys. Chem. B **1999**, 103, 9996.

18   Hicks, J. F.; Templeton, A. C.; Chen, S. W.; Sheran, K. M.; Jasti, R.; Murray, R. W.; Debord, J.; Schaaff, T. G.; Whetten, R. L. Anal. Chem. **1999**, 71, 3703.

19   Chen, S. W.; Murray, R. M.; Feldberg, S. W. J. Phys. Chem. B **1998**, 102, 9898.